Respiratory Research

RESEARCH

Open Access

The novelty of profilin 2 in regulating pyruvate kinase M2 nuclear translocation and promoting tumor angiogenesis in lung adenocarcinoma

Xiaohui Du[1], Chi Ma[2], Yingyan Wang[3], Mingxin Xu[2], Yanbin Kuang[4], Mengyun Li[2], Shuang Wen[5], Peipei He[2], Hui Zhao[6*] and Qi Wang[2*]

Abstract

Background Profilin 2 (PFN2), indispensable in all organisms, is important for cancer initiation and progression. Here, we found PFN2 highly overexpressed in tumor tissues with poor prognosis of Lung adenocarcinoma (LUAD) patients had a novel role in remodulating angiogenesis. However, the mechanism of PFN2-mediated LUAD angiogenesis remains unelucided.

Methods Immunohistochemistry and western blotting were used to detected the expression levels of related proteins in tissue or lung cancer cells. To elucidate the underlying mechanisms, we identified binding partners of PFN2 through mass spectrometry, co-immunoprecipitation, and molecular modeling techniques. Additionally, we investigated the angiogenic-promoting function of PFN2 utilizing a three-dimensional droplet-based angiogenesis model capable of simulating the tumor hypoxic microenvironment.

Results Our finding reveal that PFN2 was overexpressed in tumors compared with the adjacent nontumor tissues. Its knockdown markedly impaired the proliferation, and angiogenesis of LUAD cells via hypoxia-related NF-κB/HIF-1α signaling pathway, with vascular endothelial growth Factor (VEGF) decrease. Additionally, pyruvate kinase M2 (PKM2), a pivotal enzyme in glycolysis, is a novel binding partner of PFN2. The nuclear translocation of PKM2 was observed to be dependent on PFN2 expression and their interaction, which functionally modulates angiogenesis in lung cancer.

Conclusions Our study revealed oncogene PFN2 promoted tumor angiogenesis in LUAD through regulating PKM2 nuclear translocation, providing novel molecular therapy targets for LUAD treatment.

Keywords Profilin 2, Pyruvate kinase M2, Lung adenocarcinoma, Angiogenesis

*Correspondence:
Hui Zhao
zhaohui_dlmu@sina.com
Qi Wang
wqdlmu@163.com
[1]Department of Scientific Research Center, the Second Affiliated Hospital, Dalian Medical University, Dalian, China
[2]Department of Respiratory Medicine, the Second Affiliated Hospital, Dalian Medical University, Dalian, China
[3]Laboratory Center for Diagnostics, Dalian Medical University, Dalian, China
[4]Department of Pulmonary Medicine, Shanghai Chest Hospital, Shanghai Jiao Tong University, Shanghai, China
[5]Department of Pathology, Dalian Friendship Hospital, Dalian, China
[6]Department of Health Examination Center, the Second Affiliated Hospital, Dalian Medical University, Dalian, China

Introduction

Lung adenocarcinoma (LUAD), as one of most common lung cancer-related malignant tumors, has extremely high incidence and mortality mainly due to its inevitable aggressiveness and metastasis [1]. The significant biological processes during tumor metastasis is microvascular angiogenesis, which consists of the development of new blood vessels from pre-existing vasculature [2] and supplies adequat oxygen and nutrients to support tumor proliferation and further metastasis [3]. Accumulating evidence indicates that LUAD is prone to hypervascular metastases, suggesting antiangiogenic therapy would be a good treatment strategy. Athough anti-angiogenic drugs and combination therapy strategies [4–6] have garnered significant attention over the past few decades, poor efficacy or even drug resistance still extremely hurdles therapeutic progression. Therefore, further analysis of angiogenesis signaling involved in the growth and metastasis of LUAD would be benefit for the clinical treatment of LUAD patients.

Profilin (PFN), an ubiquitously expressed but highly conservative actin-binding protein, is crutial for multiple cellular processes, including cell proliferation and apoptosis [7], cell migration and invasion [8], cell adhesion and epithelial-mesenchymal transition (EMT), chemotherapy drug resistance [9] and angiogengsis [10]. Due to alternative splicing, there are four isoforms, Profilin 1, 2, 3 and 4. Profilin 2 (PFN2) is strongly upregulated in almost all types of tumors and highly correlated with TGF-β-mediated epithelial-mesenchymal transition (EMT) and metastasis in diverse tumors, such as colorectal cancer [11], head and neck cancer [12], and triple negative breast cancer [8]. More importantly, PFN2 could promotes small cell lung cancer (SCLC) growth, metastasis, and angiogenesis through exosomes [10]. Like its fellow family members, PFN2 possesses three domains, namely, an actin-binding domain, a phosphoinositides-binding domain, and a poly-L-proline-binding domain. Among them, the poly-L-proline-binding domain formed by the N-terminal and C-terminal helices of profiling enables PFN2 to interact with plethora proteins, making it function as a hub that control a complex network of molecular interactions [13, 14]. Therefore, we speculated PFN2 might accompany with its partner to promote angiogenesis in LUAD, yet it has not been well investigated.

Accumulating evidence indicate aerobic glycolysis helps cancer cells convert large amounts of glucose to lactate in the presence of oxygen to provide nutrients to facilitate tumor growth and metastasis. Pyruvate kinase M2 (PKM2) is a key rate-limiting enzyme in glycolysis, catalyzing the conversion of phosphoenolpyruvate (PEP) and ADP into pyruvate and ATP [15]. In the cytoplasm, PKM2 exists in either a homotetramer form that acts as a phosphotransferase [16–18], or in a low activity homodimer form that acts as a transcriptional coactivator [10, 19, 20].To response to the upstream stimulus, such as epidermal growth factor (EGF), PKM2 immediately translocates from the cytoplasm to the nucleus to act as a phosphotransferase and/or transcriptional coactivator. This dual roles render PKM2 a prominent target in tumor research [21, 22]. Moreover, PKM2 is also mainly upregulated in tumor cells, and has a positive role in tumor progression and angiogenesis.

In this study, we utilized droplet-based angiogenesis model to simulate tumor hypoxic microenvironment and revealed PFN2 potentiated PKM2-mediated angiogenesis by their protein-protein interactions, it enhancing PKM2 nuclear translocation and promoting tumor angiogenesis by hypoxia-related NF-κB/HIF-1α signaling pathway, with VEGF significantly upregulated. Based on these findings, our study illustrated the novel role of PFN2 in the regulation of angiogenesis, providing new therapy targets for LUAD treatment.

Methods

Cell culture

The human NSCLC cell lines were cultured in RPMI 1640 supplemented with 10% fetal bovine serum (FBS) and 100 U/mL penicillin/streptomycin (P/S). HEK293T cell were cultured in high glucose Dulbecco's modified Eagle medium (DMEM) supplemented with 10% FBS. Human Pulmonary Microvascular Endothelial Cells (HPMVECs, ScienCell, USA) were cultured in Endothelial Cell Medium (ScienCell) supplemented with 5% FBS and 100 U/mL P/S. Only HPMVECs at passages 6–8 were used in our experiments. The cell lines were authenticated by comparing with the STR database. All cells were cultured at 37 °C in a humidified atmosphere containing a 5% CO_2 incubator and passaged every 2–3 days.

Immunohistochemistry (IHC)

Tissue microarray of human lung adenocarcinoma and paired adjacent normal tissues (HLugA180Su06) and lung adenocarcinoma tissues (HLugA120PG01) were purchased from Shanghai Outdo Biotech Company (Shanghai, China). Sections from paraffin-embedded human or mouse tissues were stained with antibodies as indicated in the text. Staining was scored according to staining intensity (negative: 0 points; weak: 1 point; moderate: 2 points; and strong: 3 points) multiplied by the percentage of stained cells (percentage of positive cells: ≤25%: 1 point; 26–50%: 2 points; 51–75%: 3 points; ≥75%: 4 points). Scores of <6 were considered low-expression, and scores of ≥6 were considered high-expression.

Lentiviral infection and transfection

Cells were plated at a density of 4×10^5/60 mm dish, 18 h prior to transfection. Transient transfection was

performed using the Lipofectamine 2000 reagent (Invitrogen, Waltham, MA, USA) according to the manufacturer's instructions. For stable transfection, cells were infected with lentivirus and selected using puromycin (5 μg/mL) according to the manufacturer's instructions. Transfection efficiency was determined using western blotting.

Escherichia coli containing the plasmids HA-PFN2, HA-PFN2-Mus, and Flag-PKM2 were purchased from LongQian Biotech (Shanghai, China). Lentiviral and plasmid constructs for PFN2 knockdown (hU6-MCS-Ubiquitin-EGFP-IRES-puro) were purchased from GeneChem (Shanghai, China).

Cell viability and colony formation assay

Cell viability was evaluated using the cell counting kit-8 (CCK-8) assay (MedChemExpress, Monmouth Junction, NJ, USA) as per the instructions of the manufacturer. For colony formation assays, cells were plated in 6-well plates (400 cells/well) and allow to proliferate for two weeks. For colony formation, 10^3 cells were harvest and put into 6-well plates. The obtained colonies were fixed with 4% paraformaldehyde and stained with 1% crystal violet. The colonies (> 50 cells) were counted manually.

Cell apoptosis analysis

The apoptosis assay was performed using an Annexin V-FITC Apoptosis Detection Kit (C1062, Beyotime) according to the manufacturer's instructions. Stained cells were analyzed using a NovoCyte Advanteon flow cytometer (Agilent NovoCyte Advanteon).

Tube-formation assay

Matrigel with reduced growth factor (100 μL/well) was added into 48-microwell plates and placed at 37 °C for 30 min to solidify. Next, 4×10^4 human pulmonary microvascular endothelial cells (HPMVECs) were resuspended in conditioned media from different cell types and added to the microwells. Cells were incubated for 6 h.

A droplet-based tumor angiogenesis model was established as previously described[23]. Tumor cells (TCs) were 3D cultured in Matrigel, whereas HPMVECs were cultured as a monolayer. After 24 h, a coculture was formed by fusing the two cell droplets through a reciprocating horizontal movement of the capillary between the two droplets. Rhodamine phalloidin immunofluorescence staining used to assess tube formation.

Tumor xenograft model

BALB/c nude mice (7-weeks-old) were obtained from Liaoning Changsheng Biotechnology Co. Ltd. (Shenyang, China). Tumor xenografts were allowed to grow for 3 weeks. Tumors were measured every 3 days with calipers and calculated using the following formula: $a^2 \times b \times 0.5$, where a is the smallest diameter and b is the diameter perpendicular to a. The tumors were excised and weighed, and were prepared into FFPE (4 μm) for later analysis by IHC.

Western blotting analysis

Protein samples were electrophoresed on SDS-PAGE and transferred onto polyvinylidene fluoride membranes (Merck, USA), then immunoblotted with specific antibodies. The protein bands were visualized using an enhanced chemiluminescence (ECL) solution. Band intensities were quantified using the ImageJ software (NIH, Bethesda, MD, USA).

qRT-PCR

Total RNA was extracted using RNAiso Plus reagent (Takara Bio, Shiga, Japan), then converted into complementary DNA (cDNA). qPCR was performed on a LightCycler96 Real-Time System (Roche, Basel, Switzerland). The data were analyzed using the ΔΔCt method.

ELISA of human VEGF (hVEGF)

To compare the hVEGF secretion by tumor cells in 3D droplets and traditional Petri dishes, a 3D droplet array composed of A549-shNC or shPFN2 cells was generated. After culturing for 48 h, supernatants from 20 droplets were collected and diluted 50-fold with FBS-free medium in a 96-well plate. hVEGF was quantified using an ELISA kit specific for hVEGF (R&D Systems, Minneapolis, MN, USA) according to the manufacturer's protocol.

RNA-sequencing analysis

RNA-seq were performed by Novogene (Beijing, China) Co. Ltd. Differential gene expression analysis was performed using the R package limma. Genes with $|\log2FC| > 0.1$ and p-value < 0.05 were considered differentially expressed. Intersection of these differential expression genes with interested gene sets yielded the relevant differentially expressed genes. Heatmaps were constructed with the ComplexHeatmap package. Gene ontology (GO) enrichment analysis, including biological process (BP), cellular component (CC), and molecular function (MF), and Kyoto Encyclopedia of Genes and Genomes (KEGG) pathway analysis were performed using the clusterProfiler package. Enrichments with a p-value < 0.05 were considered significant.

GSEA analysis

We carried out gene set enrichment analysis (GSEA) by utilizing the GSEA software (v4.1.0) along with the Molecular Signatures Database (MSigDB). The aim was to discern whether a particular set of genes within specific Gene Ontology (GO) terms or Kyoto Encyclopedia of Genes and Genomes (KEGG) pathways exhibited

substantial differences between two groups. Briefly, we input gene expression matrix and rank genes by Signal-2Noise normalization method. Enrichment scores and p value was calculated in default parameters. GO Terms, KEGG pathways meeting this condition with|NES|>1, NOM p-val < 0.05, FDR q-val < 0.25 were considered to be different in two groups.

Co-immunoprecipitation (Co-IP)

Co-IP assays were performed using the Pierce Classic Magnetic IP/Co-IP Kit (Thermo Fisher Scientific) according to the manufacturer's protocol. Cell lysates from each sample were incubated with 10 μg of conjugated antibody, overnight at 4 °C, to form the immune complex.

Liquid chromatography with tandem mass spectrometry (LC-MS/MS) analysis of PFN2-interacting proteins

To identify PFN2-interacting proteins, co-IPed proteins were visualized after separation by electrophoresis using a Coomassie Blue Staining Kit (Beyotime, Shanghai, China). The co-IP gel and its corresponding negative gel bands were excised into five parts according to the heavy and light chains and sent to Novogene (Beijing, China) for LC-MS/MS analysis. See ESM Methods for further details.

Surface plasmon resonance (SPR) assay

The binding affinity of recombinant hPFN2 (rhPFN2) to rhPKM2 was determined using an OpenSPR biomolecular interaction analyzer with a COOH chip (SEN-AU-100-10-COOH, Nicoya, Kitchener, Ontario). The rhPKM2 protein was dissolved in 10 mM acetate buffer (pH 3.5) and immobilized onto the chip. The sensor surface was activated by injecting a mixture of 50 mM N-hydroxysuccinimide (NHS) and 200 mM 1-ethyl-3-(3-dimethylaminopropyl) carbodiimide (EDC), and blocking with 1 M ethanolamine, pH 8.5. Different concentrations of rhPFN2 (800, 400, 200, 100, 50, and 0 nM) were prepared in the running buffer (PBS). The interactions were determined at a flow rate of 20 μL/min for 240 s during the association phase, followed by 180 s for the dissociation phase at 25 °C. The data were analyzed using the TraceDrawer manager software (Uppsala, Sweden). The binding kinetic parameters were calculated by global fitting of the kinetic data from various concentrations of rhPFN2 using a one-to-one analysis model.

Computational Docking and molecular simulation

The crystal structures of PFN2 and PKM2 were obtained from the Protein Data Bank (PDB; http://www.rcsb.org/pdb/). The Rosetta software was used for protein docking, which consisted of two steps. Aggressive sampling was performed in the first step, using the centroid model. In the second step, an all-atom model was used for small-scale optimization. Blind molecular docking was performed on PFN2 and PKM2, and the active binding regions of the two proteins were set. The lowest docking energy among the 100 docking results between PFN2 and PKM2 was selected for further analysis.

Statistical analysis

Significance was calculated using GraphPad Prism software (GraphPad Software, San Diego, CA, USA). All statistical analyses were performed using data from at least three independent experiments. More than three means were compared using two- or one-way ANOVA with Bonferroni correction, and two means were compared using the unpaired Student's *t*-test of $^{*}P < 0.05$ was considered significant.

Results

Increased PFN2 expression induces poor prognosis in LUAD patients

To explore the explicit role of PFN2 in LUAD, we analyzed the PFN2 expression in 94 cases of LUAD tissues from patients pathologically diagnosed with LUAD, and 86 cases of para-carcinoma tissues, and discovered PFN2, predominantly expressed in the cytoplasm, was significantly expressed in LUAD tissues, which was also comfirmed by the H-score analysis (Fig. 1A and B). Further overall survival (OS) analyses showed that high expression of PFN2 in lung adenocarcinoma was significantly correlated with poor survival ($P < 0.0005$; Fig. 1C). Due to the prominent role of Vascular Endothelial Growth Factor (VEGF) in multiple processes such as tumor angiogenesis, lymphangiogenesis, and tumor invasiveness, we also assessed the correlation between PFN2 and VEGF in 55 lung cancer samples and observed there was a positive correlation ($R = 0.6877$; Fig. 1D-E). Collectively, these data suggest that PFN2 might promote LUAD progression via VEGF-mediated pathway and is associated with a poor prognosis in LUAD patients.

PFN2 depletion suppresses lung adenocarcinoma cells proliferation and angiogenesis

It has been reported tumor angiogenesis participated in cancer progression. To investigate whether PFN2 mediated cell proliferation and angiogenesis in LUAD, we measured its expression in different lung cancer cells and normal bronchial cells (type II alveolar epithelial cells, AT II) (Supplementary Figure S1) and slienced it in A549 cells and H1299 by lentivirus. CCK8 and colony formation assays indicated that PFN2 knockdown significantly impaired cell proliferation (Figure S2A-B). Moreover, flow cytometry analysis revealed that the apoptosis of cells increased notably after PFN2 knockdown (Figure S2C). Furthermore, we validated the relationship between PFN2 and angiogenesis through tube formation assays

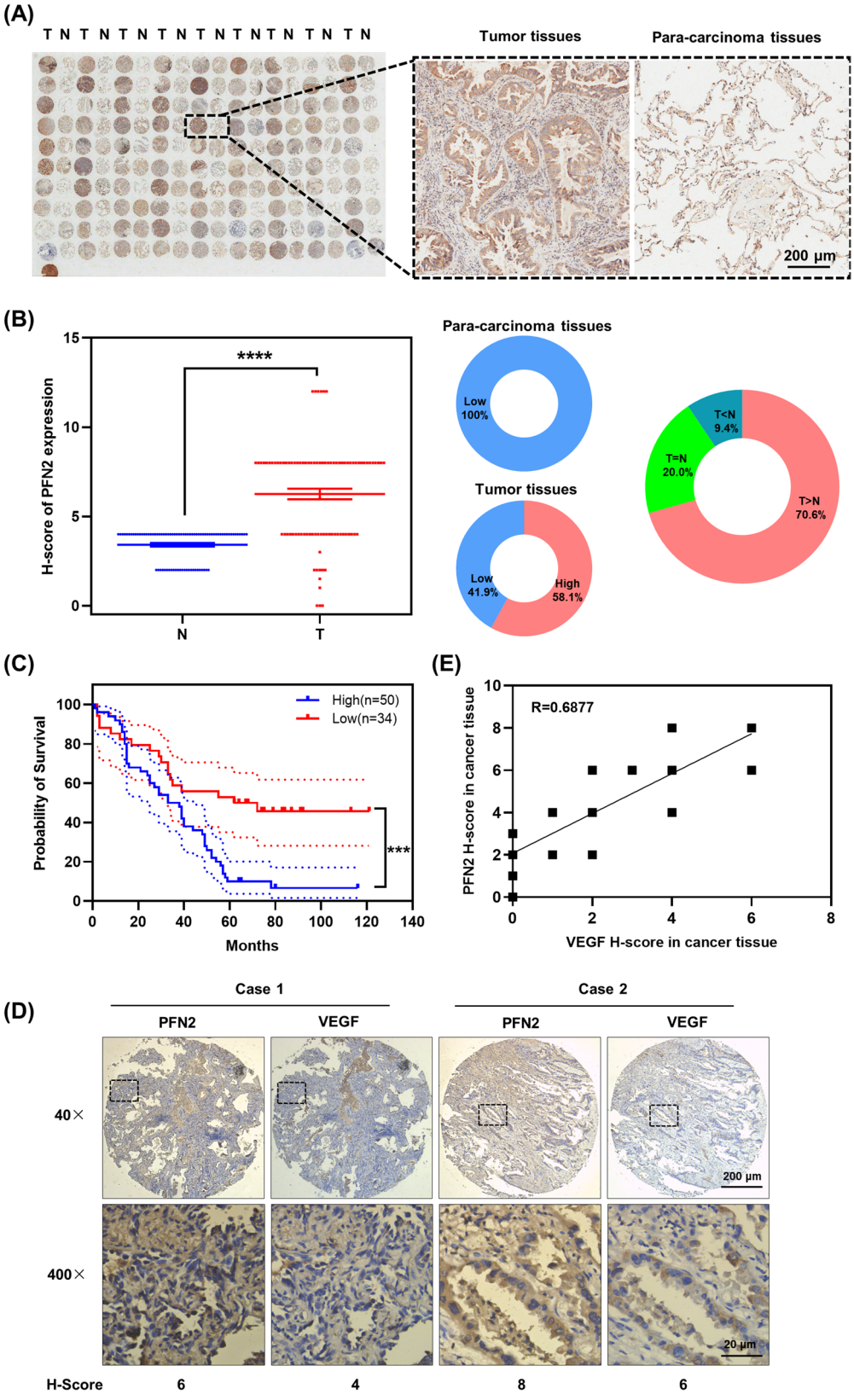

Fig. 1 Increased PFN2 expression is correlated with poor prognosis of lung adenocarcinoma patients. **(A)** The expression of PFN2 in tissue microarray was examined by Immunohistochemical staining. **(B)** H-score of PFN2 expression and analysis of the difference in expression between lung adenocarcinoma tissue and adjacent tissue. **** $p < 0.00001$. **(C)** The relationship between PFN2 expression and probability survival. 9 cases lost to follow-up were excluded. *** $p < 0.0005$. **(D)** IHC staining of PFN2 and VEGF in LUAD. **(E)** Correlation of PFN2 expression with VEGF expression of **(D)**

and vessel analyses in HPMVEC cells. In consistence with our presumption, PFN2 knockdown decreased the capacity of angiogenesis in HPMVEC cells, with reduced in vessels area ($P < 0.0001$), the total number of junctions ($P < 0.01$), and total vessels length ($P < 0.0001$) compared to the controls (Fig. 2A). To explore the potential role of PFN2 knockdown to inhibit cell proliferation in vivo, we performed subcutaneous injections of A549-shNC and A549-shPFN2#1 and #2 cells in BALB/c nude mice. The size and growth rate of the subcutaneous tumors were observed dynamically. As shown in Fig. 2B-C, PFN2 knockdown dramatically inhibited tumor growth in aspects of volume (Fig. 2B) and weight (Fig. 2C). Moreover, IHC analysis of xenograft tissue slides (Fig. 2D) demonstrated that PFN2 knockdown markedly inhibited angiogenesis identified by the classical marker gene $CD34^+$ in vivo. These results suggest that PFN2 may be necessary for the lung tumor growth and angiogenesis.

PFN2 depletion inhibits the NF-κB/HIF-1α signaling pathway

Hypoxia-inducible factors (HIFs) and the HIF-dependent cancer hallmarks angiogenesis are well-established drivers of LUAD progression, invasion, metastasis, therapy resistance, and poor prognosis [23]. Hypoxia triggers diverse transcriptional programs, including hydroxylase family (PHD1-3) downregulation and HIF-1α upregulation [24]. To further comfirm whether PFN2 mediated angiogenesis under hypoxia situation, we utilized the 3D droplet culture model to mimick the interactions between 3D tumor cells and 2D HUVECs during the formation of capillary-like structures. In this model, we cocultured 3D tumor cells and 2D HUVECs to in droplets (Fig. 3A). To validate the hypoxic state of the tumor - like tissue in the model, we used Western Blotting and IF staining in frozen sections to detect the expression of HIF-1α. We found that HIF-1α expression was enhanced in 3D droplets of lung cancer cells (Fig. 3B and C), while PHD3 was downregulated (Fig. 3B), indicating that droplet-based 3D cell culture can simulate the anoxic state of tumor tissues in vivo and can be used as a tumor-like platform for subsequent research on molecular mechanisms.

Since proangiogenic factors, such as vascular endothelial growth factor-A (VEGFA), could facilitate cancer cells to angiogenesis under hypoxia. Subsequently, we measured VEGFA mRNA and protein levels after PFN2 knockdown, and found both were decreased (Fig. 3D, E). To further clarify the effect of PFN2 knockdown on tumor angiogenesis, we collected A549-shNC, -shPFN2#1, and -shPFN2#2 cells for RNA sequencing. GSEA analysis (Fig. 3F) demonstrated a notable inhibition of the angiogenesis process following PFN2 depletion. Moreover, Fig. 3G revealed a significant downregulation of key angiogenesis-related transcription factors, including HIF-1α, PKM, and NF-κB.

Furthermore, immunoblot analyses confirmed the decreased expression of HIF-1α and p65-NF-κB, as well as their downstream effector molecules like VEGFA, Cyclin D1, and mitogen-activated protein kinase kinase 5 (MEK5) in A549 and H1299 cells after PFN2 downregulation (Fig. 3H and I), illustrating PFN2 enhances tumor growth and angiogenesis via a mechanism involving the activation of the NF-κB/HIF-1α signaling pathway and the expression of angiogenic factors.

PFN2 physically interacts with PKM2

As PFN2 was reported to be a hub molecule, it could mediate angiogenesis in a complex formation with other proteins. To uncover PFN2 molecular companion and elucidate the underlying mechanism of PFN2 in regulating lung cancer angiogenesis, we performed LC-MS/MS (Figure S4) and identified 1449 proteins accompanied with PFN2 in A549 cells. We then annotated subcellular localization information (Figure S4B) and cluster of orthologous groups of proteins (COG) (Figure S4C), revealing that the proteins bind to PFN2 are widely distributed and possess diverse functions. Among these, a band containing multiple peptides corresponding to PKM was obviously identified. Subsequently, after transfecting cells with siRNA targeting PKM (siPKM), we found that the expressions of NF-κB and HIF1α were significantly downregulated (Figure S4D). Next, we utilized Co-IP and reciprocal Co-IP analyses to validate the MS/MS-based protein identification and detect the association between PFN2 and PKM2. Briefly, pcDNA-Flag-PKM2, pcDNA-HA-Vector or pcDNA-Flag-PKM2, pcDNA-HA-PFN2 were co-transfected into HEK293T cells, respectively, followed by co-IP using anti-FLAG antibodies (Fig. 4A). Similarly, reciprocal co-IP analysis was conducted by transfecting cells with pcDNA-HA-PFN2 alone or with pcDNA-Flag-PKM2, followed by co-IP using anti-HA antibodies (Fig. 4B). Additionally, immunoblot analyses also showed that PFN2 interacted with PKM2. We further used SPR assays to measure the binding affinity between PFN2 and PKM2, in which PKM2 was immobilized on the sensor chip. A clear binding profile was observed, with a dissociation equilibrium constant of $5.06e^{-8}$ M (Fig. 4C). Immunofluorescence (IF) showed PFN2 predominantly co-localizes with PKM2 in the cytoplasm (Fig. 4D). To elucidate the binding interactions between PFN2 and PKM2, we performed molecular docking studies and found PFN2 displayed a high binding affinity to PKM2 with an estimated binding free energy of − 91.53 kcal/mol. Besides, the binding interface of PFN2 and PKM2 in the molecular dynamics simulation of 70–100 ns are shown in PartA and PartB, respectively (Fig. 4E). The amino acids at the interface

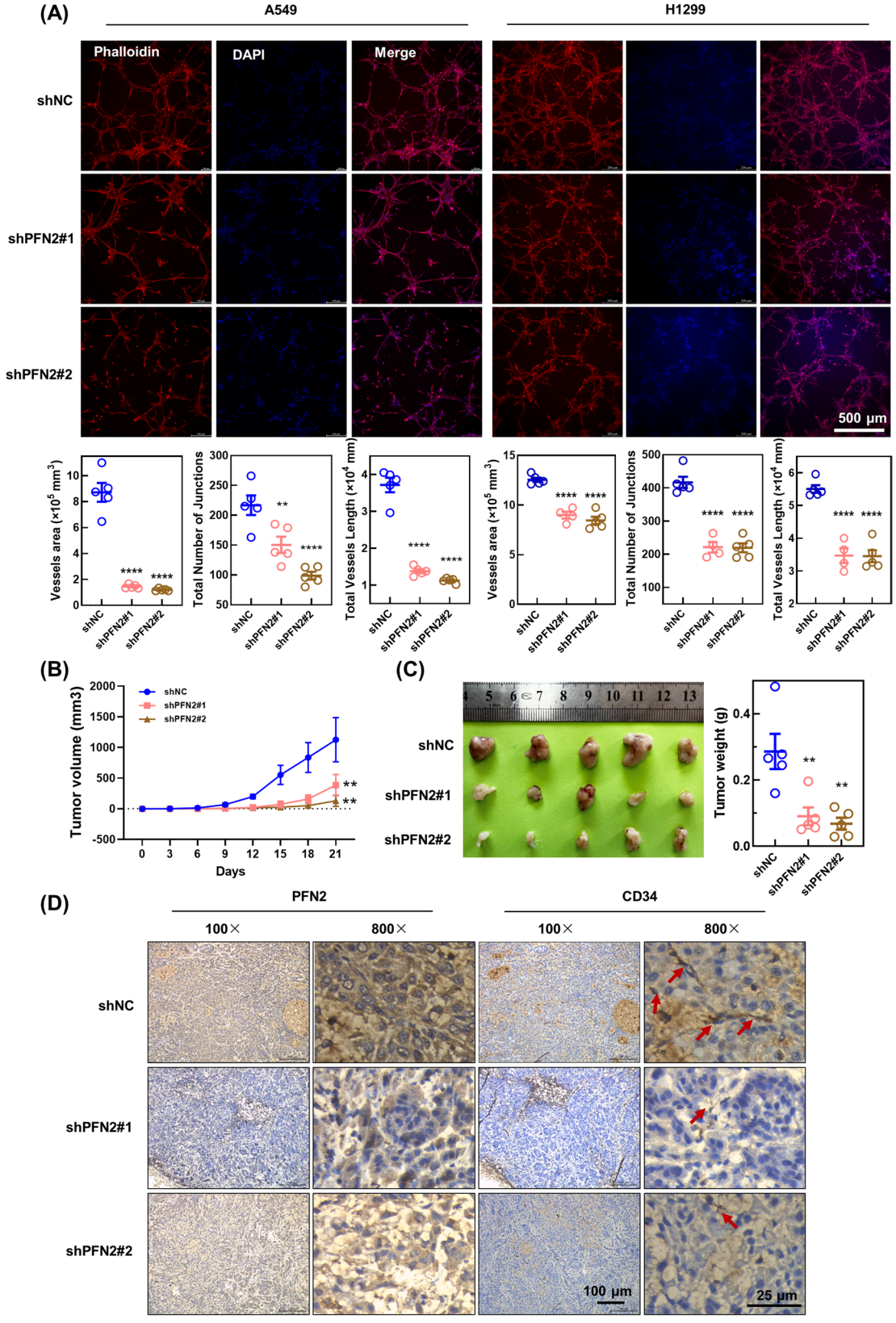

Fig. 2 PFN2 depletion inhibits tumor cell proliferation and tumor cell-induced angiogenesis. **(A)** The tube formation assay of HPMVEC-mediated angiogenesis in vitro when PFN2 knockdown and quantitative analysis. **(B)** Tumor growth curve of A549-shNC, shPFN2#1 and shPFN2#2 xenografted mice (3×10^6 cells/mouse). $^{**}P < 0.01$. **(C)** Tumor masses were weighted at the end of the expression. $^{**}P < 0.01$. **(D)** Representative images of immunohistochemical (IHC) staining for PFN2 and CD34 in xenograft tumor tissues

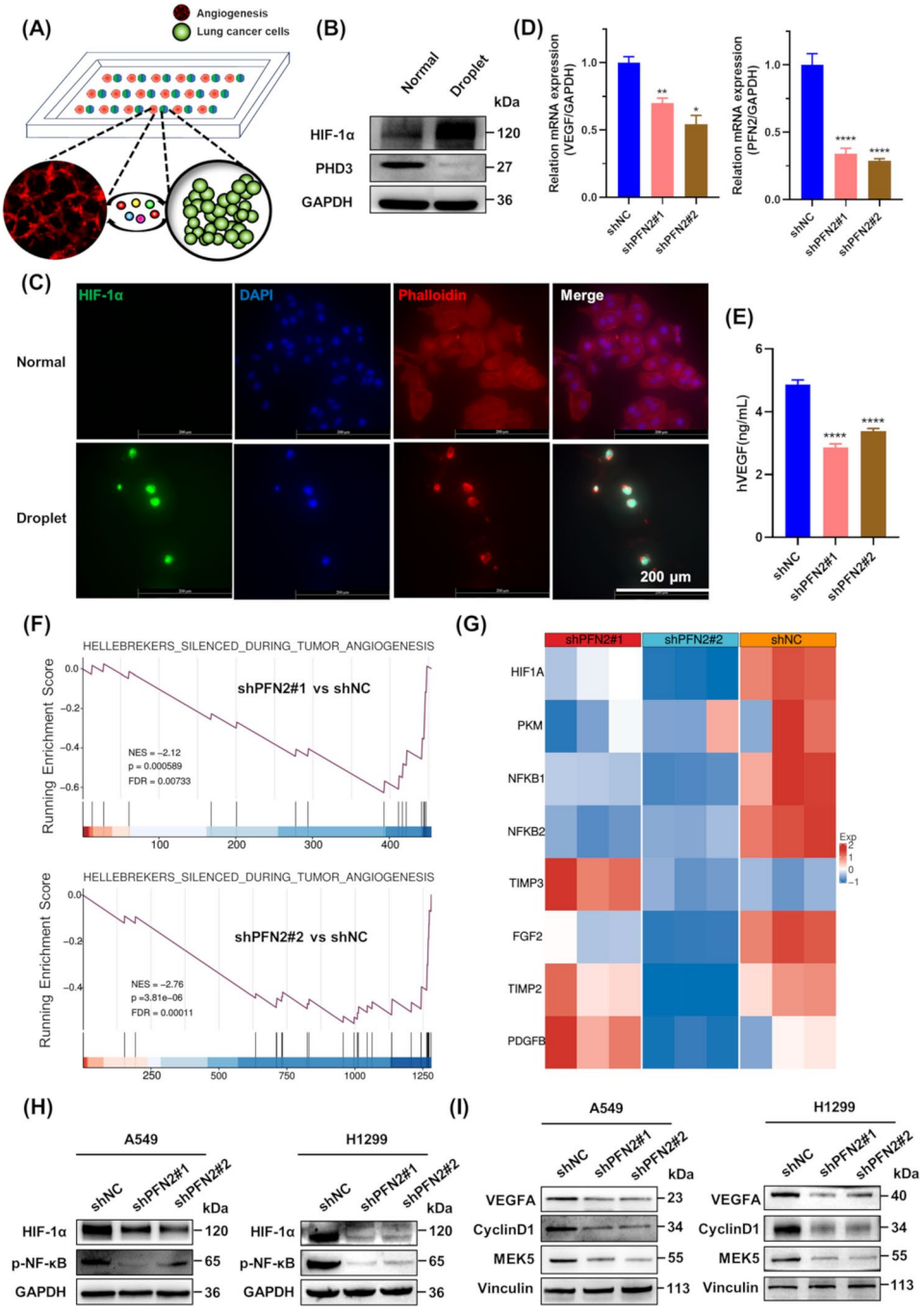

Fig. 3 PFN2 depletion inhibits the NF-κB/HIF-1α signaling pathway. **(A)** The model we built before used to culture 3D tumor cells and 2D HUVECs in droplets for angiogenesis assay. **(B)** Representative Western blot image showing the HIF-1α and PHD3 expression of A549 cultured in traditional dish and 3D droplets. **(C)** Immunofluorescent analysis of the expression of HIF-1α in A549 cultured in dish (Normal) and 3D droplets frozen sections. HIF-1α (green), Phalloidin (red) and DAPI (blue). Scale bar, 500 μm. The relative VEGF mRNA expression **(D)** and hVEGF secreted **(E)** from cells cultured in 3D droplets. ****$p < 0.0001$. **(F)** GSEA analysis of angiogenesis pathway in A549-shPFN2 cells compared to that in shNC cells. **(G)** Heatmap shows the significantly altered genes in angiogenesis pathway in A549-shPFN2 cells compared to that in shNC cells. Representative Western blot image showing the HIF-1α, p65-NF-κB **(H)** and expression of their target gene **(I)**, as VEGF, Cyclin D1 and MEK5 in the A549 cell line transfected with shPFN2 or shNC

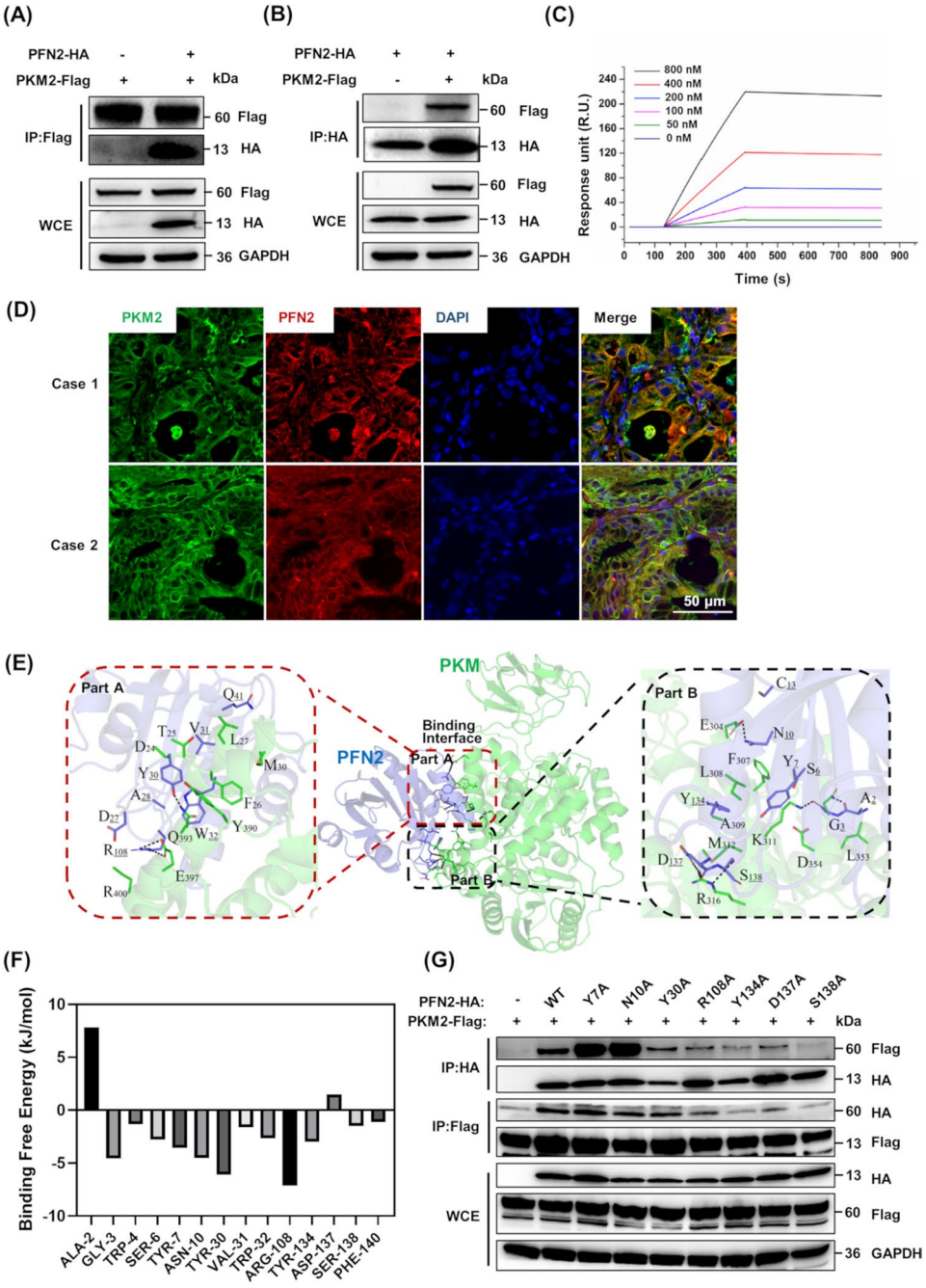

Fig. 4 PFN2 physically interacts with PKM2. Co-Immunoprecipitation (Co-IP, **A**) and reciprocal co-IP analysis **(B)** the interaction between PFN2 and PKM2 in the HEK293 cells as indicated. **(C)** Interactions between PFN2 and PKM2 were determined by SPR assay. **(D)** Immunofluorescence analysis of PKM2 (Green) and PFN2 (Red) expression in tumor tissues. **(E)** The binding modes of PFN2 (blue) and PKM2 (green). Magnified image (left and right) showed two parts of the binding interface. **(F)** Molecular Mechanics/Generalized Born Surface Area (MM/GBSA) free energy decomposition analysis of the total binding free energy per residue for the PFN2/ PKM2 system. The key residues for ligand binding are labeled. **(G)** HEK293T cells were co-transfected with eukaryotic plasmids expressing full-length wild-type Flag-PKM2 and mutant variants of HA-PFN2, and analyzed by Co-IP and western blotting using antibodies against Flag and HA

between the two proteins form a relatively dense binding network. For example, PKM2 forms four hydrogen bonds with residues A2, N10, Y30, and S138 of PFN2 and two salt bridges with residues R108 and D137 at the interaction interface. Moreover, MM/GBSA free energy decomposition analysis showed that residues Y7, N10, Y30, R108, Y134, D137 and S138 significantly contributed (< -1 kcal/mol) to the combination between PFN2 and PKM2 (Fig. 4F).

To figure out which binding sites were crucial, we mutated these residues in the PFN2 binding interface and transfected HEK293T cells with plasmids harboring these mutations for Co-IP analyses. Except for single point mutation Y30A, we found R108, Y134, D137, and S138 sites replaced by alanine significantly weakened the binding between PFN2 and PKM2, particularly Y134A and S138A. As for Mutations Y7A and N10A, they appeared to block the breakdown of the complex (Fig. 4G). Taken together, these results confirm that PFN2 is physically associated with PKM2 and that the most critical interaction region in PFN2 resides in the C-terminal region (residues 108–138).

PFN2 regulates the expression and nuclear translocation of PKM2

It has reported that PKM2 regulates the final step of glycolysis by transferring a phosphate group from PEP to ADP to produce pyruvate and adenosine triphosphate (ATP), which was necessary for cancer cells to maintain enough nutrients and facilitate angiogenesis [25]. To investigated whether PFN2 impacts lung cancer growth and angiogenesis by regulating PKM2. We first determined the expression levels of PKM2 in shPFN2 cells and found that PKM2 expression was downregulated (Fig. 5A). To investigate whether PFN2 affects the nuclear localization of PKM2, we assessed the nuclear and cytosolic distributions of PKM2 in shNC- and shPFN2-transfected cells. Western blotting analysis of nuclear and cytosolic fractions from shPFN2-expressing cells revealed a significant decrease in the nuclear PKM2 signal in shPFN2 cells compared to that in shNC cells (Fig. 5B). Phosphorylation of PKM2 at S37 mediated by ERK1/2 is known to induce translocation of PKM2 to the nucleus [17, 26]. Admittedly, Our results confirmed PFN2 knockdown led to impaired phosphorylation of PKM2 S37 (Fig. 5C).

PKM2 has been demonstrated to translocate into the nucleus and participate in transcriptional activation in response to epidermal growth factor (EGF) stimulation. We pretreated shPFN2 cells with or without EGF. Western blotting of the cytoplasmic and nuclear fractions (Fig. 5D) and IF (Fig. 5E) analysis showed PKM2, a primarily cytosolic protein, translocated into the nucleus upon EGF stimulation in shNC cells. However, PKM2 nuclear translocation was completely impaired in shPFN2 cells even when PKM2 expression were increased and S37 phosphorylation were restored after EGF treatment. Taken together, these results suggest that PFN2 regulates PKM2 nuclear translocation in other decisive ways besides regulating the expression of ERK.

Binding of PFN2 to PKM2 is required for nuclear translocation of PKM2 and affects lung cancer angiogenesis

The aforementioned results led us to question whether binding of PFN2 to PKM2 was necessary for the nuclear translocation of PKM2. To answer this, we rescued PFN2 in A549-shPFN2 cells by transfected with Vector, PFN2 wide-type and mutants (Y134A, S138A) lentivirus. Analysis of whole-cell extracts revealed that the PKM2 expression and phosphorylation of PKM2-Ser37 significantly recover in cells expressing either wild-type or mutant-rescued PFN2 (Fig. 6A). Despite this, the nuclear translocation of PKM2 in cells rescued with PFN2 Y134A or S138A follows a similar reduction as observed in Res-Vector cells (Fig. 6B). A similar PKM2 nuclear translocation were also observed by IF analysis (Fig. 6C). We also explored the effect of these PFN2 rescues on angiogenesis and similarly found that PFN2 rescues restored tube formation in HPMVEC cells, while rescuing of PFN2 Y134A did not (Fig. 6D). These results indicate that the interaction between PKM2 and PFN2 is necessary for the nuclear localization of PKM2, as demonstrated by impaired translocation of PKM2 elicited by PFN2 binding site mutations, which in turn affects angiogenesis.

Discussion

PFN2 is a crucial member of the profilin family of actin-binding proteins. In this study, we identify, for the first time, PFN2 as a novel PKM2-interacting protein and unveil its regulatory role in PKM2 nuclear translocation and tumor angiogenesis in LUAD progression (Fig. 7), providing a novel ideas for further application of PFN2 as a therapeutic target against tumor angiogenesis and enhancing clinical trials of lung cancer.

Recent studies have reported that PFN2 is abnormally expressed in lung-related cancers. For instance, PFN2 has been observed to be significantly overexpressed in non-small cell lung cancer (NSCLC). Li et al. [27] attributed PFN2 upregulation to circular RNA ataxin 7. Besides, the oncogenic circular RNA SLC16A1 [28] and microRNA-30a-5p [29] could also regulate PFN2 expression to mediate NSCLC progression or EMT. Tang et al. found that PFN2 promotes growth and metastasis of lung cancer by stimulating TGF-β1-mediated EMT, as well as VEGF and connective tissue growth factor (CTGF) through epigenetic mechanisms [30]. VEGF and CTGF are important vascular growth factors that can effectively promote vascular regeneration. However, investigations on LUAD angiogenesis or molecular mechanisms underlying PFN2-mediated tumor angiogenesis are relatively limited.

Numerous PFN2-binding proteins have been reported and are characterized by high heterogeneity, such as Vasodilator-stimulated phosphoprotein (VASP) [31],

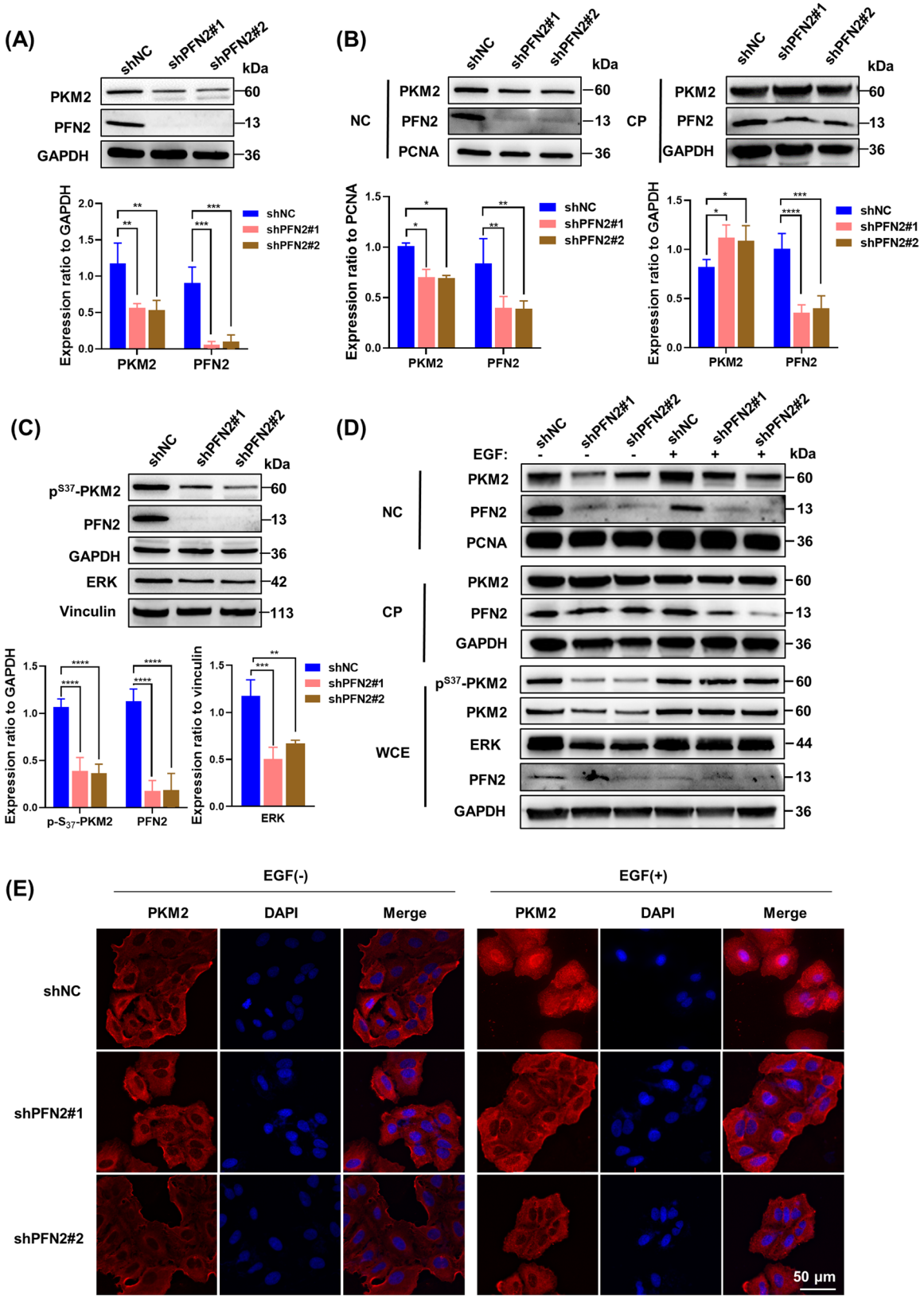

Fig. 5 PFN2 regulates the expression and nuclear translocation of PKM2. The protein level of PKM2 in whole-cell lysates **(A)** or nuclear and cytosolic fractions **(B)** in shNC- and shPFN2-transfected cells. **(C)** The expression of PKM2 nuclear translocation-related protein were analyzed by western blotting. The shNC- and shPFN2-transfected cells were treated with or without EGF (100 ng/ml) for 6 h, western blotting **(D)** and Immunofluorescence analyses **(E)** were performed as indicated. PKM2 (red), DAPI (blue)

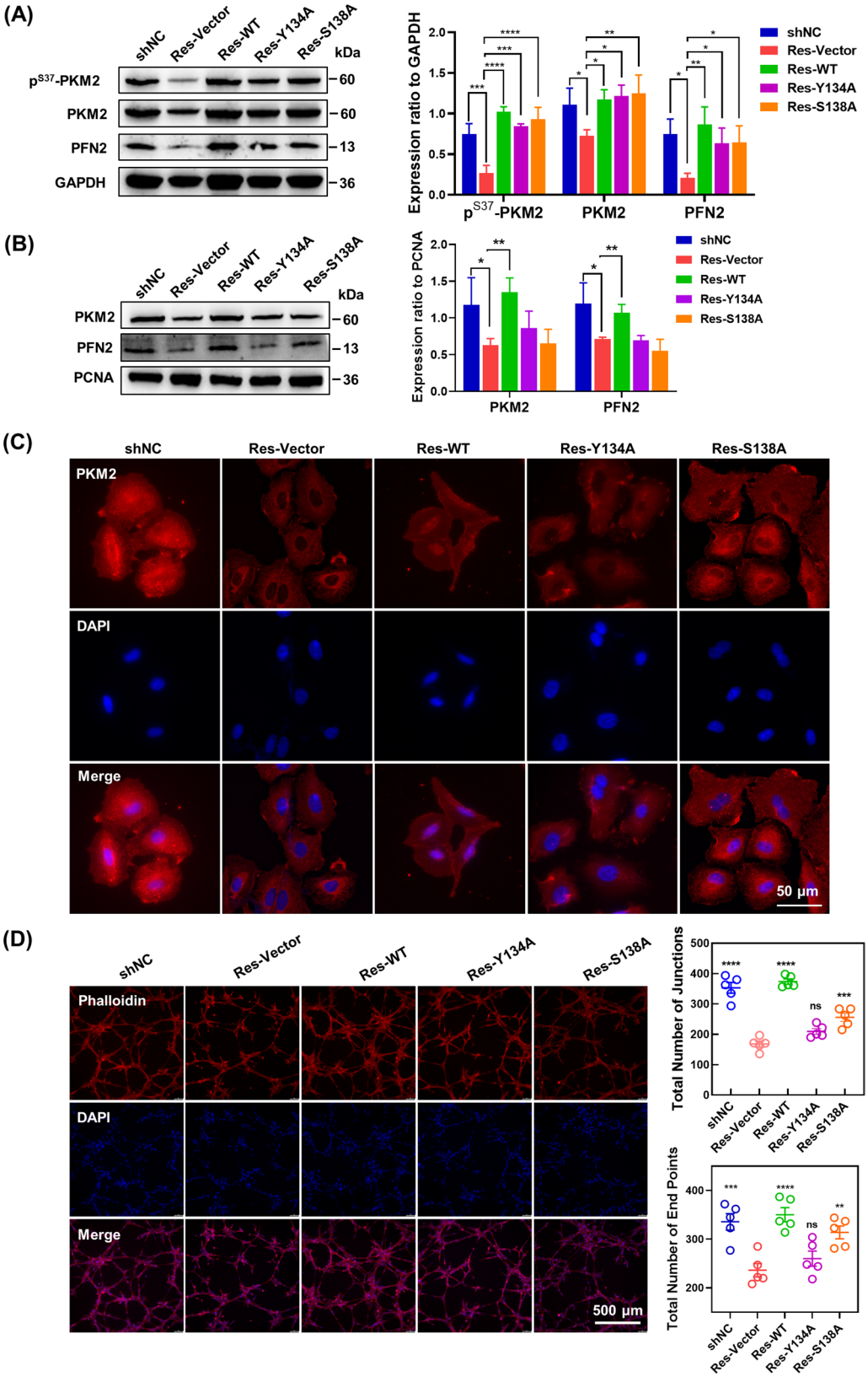

Fig. 6 Binding of PFN2 to PKM2 is required for nuclear translocation of PKM2 and regulating lung cancer angiogenesis. Western blot analysis of proteins in whole-cell extracts **(A)** or nuclear fractions **(B)** as indicated in PFN2 rescue cells. **(C)** Immunofluorescence analyses of PKM2 (red) and DAPI (blue) in PFN2 rescue cells. **(D)** The tube formation assay of HPMVEC-mediated angiogenesis in vitro when PFN2 rescue. Phalloidin (red) and DAPI (blue)

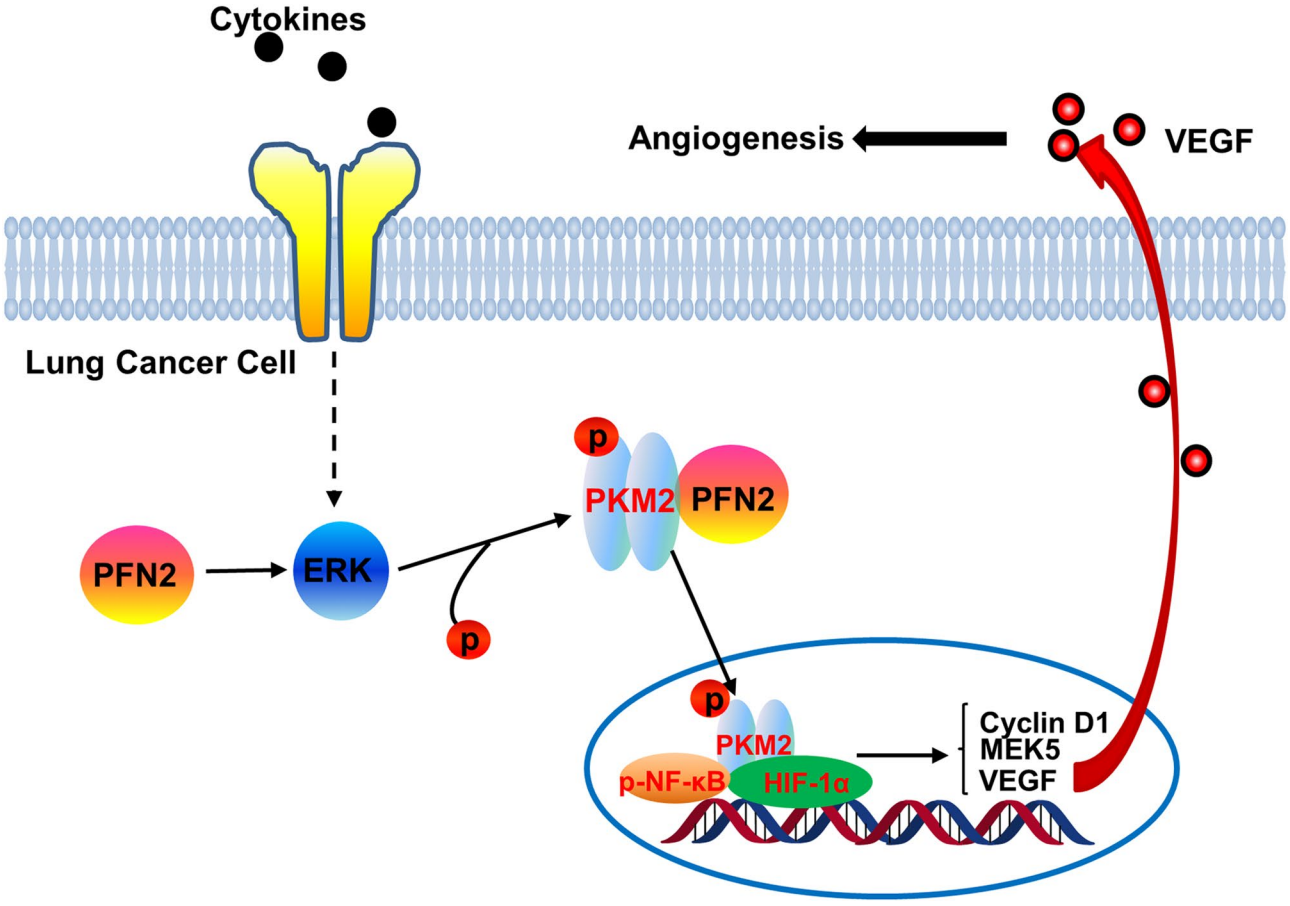

Fig. 7 A schematic illustrating the mechanism by which PKM2 nuclear translocation and induce angiogenesis

Survival of Motor Neuron (SMN) protein [32], Dynamin 1 [33], Rho-associated kinase (ROCK) [34], N-terminal acetyltransferase NAA80 [33], Histone deacetylase HDAC1 [30, 35], and Retinoic acid receptor alpha subtype (RARα) [36]. However, PFN2 was tissue-specific with different binding ligands, indicating that PFN2 have varied biological functions but are still unresolved. In our work, hundreds of potential PFN2 interactors were detected. Most of these were binding proteins, which were involved in translation, posttranslational modification, protein turnover progresses and functioned as chaperones, including fatty acid-binding protein 5, polypyrimidine bundle-binding protein, polyadenylate-binding protein, S100 calcium-binding protein, and Hsp90. These indicate that PFN2 interferace could be an effective node for inhibiting these signaling networks, especially preventing tumorigenesis.

PKM2 plays a vital role in tumor glycolysis [25], oxidative stress [37], and angiogenesis [25, 38] in various tumors. Here, we report a regulatory effect mediated by PFN2 on lung cancer angiogenesis via its combination with PKM2. Interferace with their interaction results in reduced nuclear translocation of PKM2, thus affecting angiogenesis. In addition, mutation of PFN2 at Y134 or S138 residue abrogates the PFN2-dynamin interaction and inhibits endocytosis [39], which has been suggested as a new strategy for tumor immunotherapy [40]. However, if these two PFN2 sites were targeted simultaneously, unexpected effects may occur. This indicates that additional research is needed to uncover the complex regulatory effects of PFN2 in tumor cells, which may elicit the development of multi-effect antitumor drugs targeting PFN2.

Hypoxia is a critical feature of the microenvironment of all solid tumors and a key driver of tumor angiogenesis. However, most hypoxia-regulated investigations derived from in vitro studies, where tumor cells are subjected to short periods of low oxygen concentrations (1% O_2) or chemical hypoxia mimetics, such as cobalt chloride [41, 42]. Whereas, intratumoral hypoxia in vivo could truely exhibit distinct patterns of gene expression and drug responses [43]. In this study, we employed our previously developed droplet-based tumor angiogenesis model to mimick hypoxic microenvironments and investigate anoxic-related genes. We successfully identified HIF-1α is activated, validating the effectiveness of our model.

Additionally, immune cells can be integrated into models to study cellular interactions and their molecular mechanisms under hypoxic environments.

Conclusions

In summary, we discover the novel role of PFN2 on lung cancer angiogenesis via its binding to PKM2. Inhibition of PFN2 causes abnormal vascular functions, including decreasing vessel number and tumor growth in vitro. Notebly, we utilized 3D droplet-based angiogenesis model to mimick hypoxic microenvironments and provide a new insight of PFN2 regulating PKM2 nuclear translocations and influencing hypoxia-related NF-κB/HIF-1α downstream pathway in vivo. PFN2 knockdown interferes with PKM2 S37 phosphorylation via ERK1/2, which inhibited PKM2 nuclear translocation, and disrupted the interaction between PFN2 and PKM2, thus inhibiting tumor angiogenesis. Therefore, our assay unveiled the novel PFN2-PKM2-angiogenic factor signaling axis involved in LUAD tumor angiogenesis and provided a promising target for LUAD treatment as well.

Supplementary Information

The online version contains supplementary material available at https://doi.org/10.1186/s12931-025-03281-y.

Supplementary Material 1

Supplementary Material 2

Acknowledgements
The authors would like to thank Novogene co. ltd and wayen biotechnologies shanghai inc for excellent technical support and Dr. Xuena Chen for the linguistic editing of the manuscript.

Author contributions
D.X.H. and Z.H. designed, performed and analyzed experiments and contributed to writing the manuscript. M.C., L.M.Y and H.P.P. prepared Figs. 4 and 5. X.M.X. and W.Y.Y. analyzed data. W.S. prepared Figs. 1 and 2. K.Y.B. provided protocols and technical input. W.Q. and D.X.H. conceived and supervised the project, designed, and analyzed experiments, and revise the manuscript. All authors reviewed the manuscript.

Funding
This work was funded in part by the Natural Science Foundation of China (81903185, 82027805, 81972916 and 81703087), the Talent Innovation Support Plan of Dalian (2021RQ008), Liaoning Revitalization Talents Program (XLYC2002013), Project of Education Department of Liaoning Province (JYTZD2023045, LJKZ0833).

Data availability
No datasets were generated or analysed during the current study.

Declarations

Ethics approval and consent to participate
Approval of the research protocol by an Institutional Reviewer Board: The clinical sample research protocol were approved by the Ethics Committee of Shanghai Outdo Biotech Company (SHYJS-CP-1904008 and SHYJS-CP-1510004).

Consent for publication
Not applicable.

Competing interests
The authors declare no competing interests.

Animal studies
This study was performed in line with the principles of the Declaration of Helsinki. Approval was granted by the Ethics Committee of Dalian Medical University (AEE23117).

Clinical trial registration
Not applicable. This study is NOT a clinical trial, it does not report the results of a health care intervention on human participants.

Received: 27 September 2024 / Accepted: 16 May 2025
Published online: 29 May 2025

References

1. Siegel RL, Giaquinto AN, Jemal A. Cancer statistics, 2024. CA Cancer J Clin. 2024;74(1):12–49.
2. Risau W. Mechanisms of angiogenesis. Nature. 1997;386(6626):671–4.
3. Folkman J. Role of angiogenesis in tumor growth and metastasis. Semin Oncol. 2002;29(6 Suppl 16):15–8.
4. Roviello G, et al. Apatinib: A novel receptor tyrosine kinase inhibitor for the treatment of gastric cancer. Cancer Lett. 2016;372(2):187–91.
5. Le X, Dual EGFR-VEGF, Pathway Inhibition, et al. A promising strategy for patients with EGFR-Mutant NSCLC. J Thorac Oncol. 2021;16(2):205–15.
6. Yi M, et al. Synergistic effect of immune checkpoint Blockade and anti-angiogenesis in cancer treatment. Mol Cancer. 2019;18(1):60.
7. Li H et al. PFN2a suppresses C2C12 myogenic development by inhibiting proliferation and promoting apoptosis via the p53 pathway. Cells, 2019. 8(9).
8. Ling Y, et al. Profilin 2 (PFN2) promotes the proliferation, migration, invasion and epithelial-to-mesenchymal transition of triple negative breast cancer cells. Breast Cancer. 2021;28(2):368–78.
9. Zhao Y, et al. Circle RNA circABCB10 modulates PFN2 to promote breast Cancer progression, as well as aggravate radioresistance through facilitating glycolytic metabolism via miR-223-3p. Cancer Biother Radiopharm. 2021;36(6):477–90.
10. Cao Q, et al. Profilin 2 promotes growth, metastasis, and angiogenesis of small cell lung cancer through cancer-derived exosomes. Aging. 2020;12(24):25981–99.
11. Zhang H, et al. Loss of profilin 2 contributes to enhanced epithelial-mesenchymal transition and metastasis of colorectal cancer. Int J Oncol. 2018;53(3):1118–28.
12. Zhou K, et al. Profilin 2 promotes proliferation and metastasis of head and neck Cancer cells by regulating PI3K/AKT/β-Catenin signaling pathway. Oncol Res. 2019;27(9):1079–88.
13. Metzler WJ, et al. Identification of the poly-L-proline-binding site on human profilin. J Biol Chem. 1994;269(6):4620–5.
14. Mahoney NM, et al. Profilin binds proline-rich ligands in two distinct amide backbone orientations. Nat Struct Biol. 1999;6(7):666–71.
15. Lv L, et al. Mitogenic and oncogenic stimulation of K433 acetylation promotes PKM2 protein kinase activity and nuclear localization. Mol Cell. 2013;52(3):340–52.
16. Wiese EK, Hitosugi T. Tyrosine kinase signaling in Cancer metabolism: PKM2 paradox in the Warburg effect. Front Cell Dev Biol. 2018;6:79.
17. Yang W, et al. Nuclear PKM2 regulates β-catenin transactivation upon EGFR activation. Nature. 2011;480(7375):118–22.
18. Yang W, et al. PKM2 phosphorylates histone H3 and promotes gene transcription and tumorigenesis. Cell. 2012;150(4):685–96.
19. Morfouace M, et al. Control of glioma cell death and differentiation by PKM2-Oct4 interaction. Cell Death Dis. 2014;5(1):e1036.
20. Damasceno LEA et al. PKM2 promotes Th17 cell differentiation and autoimmune inflammation by fine-tuning STAT3 activation. J Exp Med, 2020. 217(10).
21. Ma WK, et al. ASO-Based PKM Splice-Switching therapy inhibits hepatocellular carcinoma growth. Cancer Res. 2022;82(5):900–15.
22. Wu S, et al. Therapeutic m(6)A eraser ALKBH5 mRNA-Loaded Exosome-Liposome hybrid nanoparticles inhibit progression of colorectal Cancer in preclinical tumor models. ACS Nano. 2023;17(12):11838–54.
23. Yuan X, et al. Targeting hypoxia-inducible factors: therapeutic opportunities and challenges. Nat Rev Drug Discov. 2024;23(3):175–200.

24. Jing X, et al. Role of hypoxia in cancer therapy by regulating the tumor microenvironment. Mol Cancer. 2019;18(1):157.
25. Zhang W, et al. FOXM1D potentiates PKM2-mediated tumor Glycolysis and angiogenesis. Mol Oncol. 2021;15(5):1466–85.
26. Yang W, et al. ERK1/2-dependent phosphorylation and nuclear translocation of PKM2 promotes the Warburg effect. Nat Cell Biol. 2012;14(12):1295–304.
27. Li D, et al. Downregulation of circATXN7 represses non-small cell lung cancer growth by releasing miR-7-5p. Thorac Cancer. 2022;13(11):1597–610.
28. Jin M, et al. Oncogenic circ-SLC16A1 promotes progression of non-small cell lung cancer via regulation of the miR-1287-5p/profilin 2 axis. Cell Mol Biol Lett. 2024;29(1):43.
29. Yan J, Ma C, Gao Y. MicroRNA-30a-5p suppresses epithelial-mesenchymal transition by targeting profilin-2 in high invasive non-small cell lung cancer cell lines. Oncol Rep. 2017;37(5):3146–54.
30. Tang YN, et al. Epigenetic regulation of Smad2 and Smad3 by profilin-2 promotes lung cancer growth and metastasis. Nat Commun. 2015;6:8230.
31. Reinhard M, et al. The proline-rich focal adhesion and microfilament protein VASP is a ligand for profilins. Embo J. 1995;14(8):1583–9.
32. Giesemann T, et al. A role for polyproline motifs in the spinal muscular atrophy protein SMN. Profilins bind to and colocalize with Smn in nuclear gems. J Biol Chem. 1999;274(53):37908–14.
33. Witke W, et al. In mouse brain profilin I and profilin II associate with regulators of the endocytic pathway and actin assembly. Embo J. 1998;17(4):967–76.
34. Ree R, et al. PFN2 and NAA80 cooperate to efficiently acetylate the N-terminus of actin. J Biol Chem. 2020;295(49):16713–31.
35. Chen WH, et al. FMNL1 mediates nasopharyngeal carcinoma cell aggressiveness by epigenetically upregulating MTA1. Oncogene. 2018;37(48):6243–58.
36. Andriamoratsiresy D, et al. PFN2a, a new partner of RARα in the cytoplasm. Biochem Biophys Res Commun. 2018;495(1):846–53.
37. Liang J, et al. Mitochondrial PKM2 regulates oxidative stress-induced apoptosis by stabilizing Bcl2. Cell Res. 2017;27(3):329–51.
38. Azoitei N, et al. PKM2 promotes tumor angiogenesis by regulating HIF-1α through NF-κB activation. Mol Cancer. 2016;15:3.
39. Sangokoya C, Blelloch R. MicroRNA-dependent Inhibition of PFN2 orchestrates ERK activation and pluripotent state transitions by regulating endocytosis. Proc Natl Acad Sci U S A. 2020;117(34):20625–35.
40. Chew HY, et al. Endocytosis Inhibition in humans to improve responses to ADCC-Mediating antibodies. Cell. 2020;180(5):895–e91427.
41. Liu X et al. HIF-1-regulated expression of calreticulin promotes breast tumorigenesis and progression through Wnt/β-catenin pathway activation. Proc Natl Acad Sci U S A, 2021. 118(44).
42. Bao L, et al. Methylation of hypoxia-inducible factor (HIF)-1α by G9a/GLP inhibits HIF-1 transcriptional activity and cell migration. Nucleic Acids Res. 2018;46(13):6576–91.
43. Godet I, et al. Fate-mapping post-hypoxic tumor cells reveals a ROS-resistant phenotype that promotes metastasis. Nat Commun. 2019;10(1):4862.

Publisher's note